Journal of Astronomical Telescopes, Instruments, and Systems

AstronomicalTelescopes.SPIEDigitalLibrary.org

Upgrade of the 30-m x-ray pencil beam line at the Institute of Space and Astronautical Science

Takayuki Hayashi
Toshiki Sato
Naomichi Kikuchi
Sho Kurashima
Nozomi Nakaniwa
Takuro Sato
Ryo Iizuka
Yoshitomo Maeda
Manabu Ishida

SPIE.

Upgrade of the 30-m x-ray pencil beam line at the Institute of Space and Astronautical Science

Takayuki Hayashi,[a,b,*] Toshiki Sato,[a,c] Naomichi Kikuchi,[a,c] Sho Kurashima,[a,c] Nozomi Nakaniwa,[a,c] Takuro Sato,[a,c] Ryo Iizuka,[a] Yoshitomo Maeda,[a] and Manabu Ishida[a,c]
[a]Institute of Space and Astronautical Science, Japan Aerospace Exploration Agency, 3-1-1 Yoshinodai, Chuo-ku, Sagamihara, Kanagawa 252-5210, Japan
[b]Nagoya University, Furo-Cho, Chikusa-ku, Nagoya 464-8602, Japan
[c]Tokyo Metropolitan University, Department of Physics, 1-1 Minami-Osawa, Hachioji, Tokyo 192-0397, Japan

Abstract. The 30-m x-ray pencil beam line at the Institute of Space and Astronautical Science has been upgraded. The vacuum chamber has been replaced by a new cylindrical chamber of diameter 1.8 m and length 11.3 m. Stages on which a telescope and detectors had been mounted were also replaced. At the same time, a new charge-coupled device consisting of 1240×1152 pixels of size 22.5×22.5 μm^2 was introduced. The detector stage can be moved along the x-ray beam in the vacuum chamber, which enables us to vary the distance between the sample and the detectors from 0.7 to 9 m. The two stages can be moved in a square region 500×500 mm^2 in the plane normal to the x-ray beam. The pitching of moving axes of Y direction (horizontal and normal to the beam) of the sample and the detector stages is somewhat large, but does not exceed 60 arc sec. The pitching of the other axes and the yawing of all the axes are less than 30 arc sec. As for rolling, we could obtain only the upper limits because of the difficulty in measuring them. The upper limit of the Z direction (vertical and normal to the beam) of the detector stage moving axis is somewhat large and is about 60 arc sec, and those of the other axes are less than 30 arc sec. A summary of the beam line performance is presented. Soon after the upgrade, the ASTRO-H Soft X-ray telescopes were calibrated in this beam line. © *The Authors. Published by SPIE under a Creative Commons Attribution 3.0 Unported License. Distribution or reproduction of this work in whole or in part requires full attribution of the original publication, including its DOI.* [DOI: 10.1117/1.JATIS.1.4.044004]

Keywords: x-ray beam line facility; x-ray optics; ASTRO-H.

Paper 15023P received May 14, 2015; accepted for publication Oct. 23, 2015; published online Nov. 25, 2015.

1 Introduction

Because of their great distance, x-rays emitted by celestial objects are nearly parallel by the time they arrive at earth. While it is preferred to calibrate the telescope using a parallel beam of x-rays with a diameter equal to that of the telescope, this is extremely difficult to achieve in practice.

An alternative method is to use a large-size diverging beam from a small x-ray source located at a distance much further than the focal length of the sample telescope. In this case, the telescope is fully illuminated by the beam while the focal length at the finite source becomes a little longer due to the lens equation. This method successfully works for telescopes whose angular resolution is extremely good such as the Chandra high-resolution mirror assembly.[1]

X-ray telescopes of a tightly nested type were mounted on the Suzaku satellite. For the tightly nested type of X-ray telescopes, the half-power diameter (HPD) of the encircled energy function and the mirror effective area cannot be correctly measured with a large diverging beam. For parallel light, the full area of the primary and secondary reflectors is effective. However, due to the tight nesting of the reflectors of the tightly nested type, diverging beams cannot illuminate the lower portion of the primary reflectors because of shadowing by the inner reflectors. Moreover, the reflected x-rays from the upper portion of the primary reflectors do not arrive at the secondary reflectors because of the finite incident angle of the diverging beam. Consequently, the edges of the reflectors contribute less to the focusing of the focal plane image when a diverging beam is utilized for the measurement. For example, the diverging angle at the outermost reflector reaches about 5.3 arc min for the outermost reflector of ATRO-E2 even for utilizing Panter facility, whose distance between the source and sample is 130 m.[2] A beam with a much smaller divergence is required for the calibration of these telescopes.

The 30-m x-ray pencil beam line at the Institute of Space and Astronautical Science (ISAS) is a unique beam line that provides a pencil-beam raster-scan for a diameter of up to 40 cm.[3] The beam line is characterized by a pencil beam with a small diverging angle of <20 arc sec for the 2×2 mm^2 beam size. It also has two synchronized moving stages on which an x-ray telescope and two detectors are mounted. This feature allows us to illuminate the entire aperture of the mounted telescope with a pencil beam of small divergence, which provides an accurate measure of both the effective area and the global image quality (HPD).

In fact, it was utilized for ground-based calibrations of the x-ray telescopes onboard the ASTRO-D (ASCA[4]), ASTRO-E,[5] InFOCμS,[6] and ASTRO-E2 (Suzaku)[7] satellites as well as for performance evaluations of many of the trial models. The response functions of the x-ray telescopes onboard satellites were developed by reference to the data taken in this beam line.

The focal length and the aperture of different x-ray telescopes are diverse, each being optimized for a given scientific goal. For example, the focal length of the soft x-ray telescope (SXT) of

*Address all correspondence to: Takayuki Hayashi, E-mail: thayashi@astro.isas.jaxa.jp

ASTRO-H is 5600 mm,[8] which was longer than the maximum limit of the distance between the mounted telescope and the detectors (4750 mm) in the ISAS x-ray beam line. Conversely, the lower limit of the distance (3500 mm) was longer than, e.g., the 700 mm of the focal length of the Four-Stage X-ray Telescope (FXT) of the Diffuse Intergalactic Oxygen Surveyor satellite.[9] Moreover, the aperture of the SXT is 450 mm, which was also larger than the range in which the stages could move (400 mm).

Due to this wide variation in aperture and focal length (and, thus, calibration requirements), we upgraded the ISAS x-ray beam line after 2011, replacing it with a vacuum chamber and stage system. At present, a telescope with an aperture 45 cm in diameter and with a focal length up to 9 m can be fully scanned with a pencil beam. At the same time, a new charge-coupled device (CCD) consisting of 1240×1152 pixels of size $22.5 \times 22.5\ \mu m^2$ was introduced. Moreover, a housekeeping system monitoring the temperature and the contamination in the vacuum chamber was also newly installed for safety operations while measuring samples.

2 Institute of Space and Astronautical Science Upgraded Beam Line Systems

2.1 *Vacuum Chamber*

A schematic view of the beam line is shown in Fig. 1. A Cartesian coordinate system of the ISAS beam line is set up with the x-ray beam direction defining the $+X$ axis and the direction opposite to the direction of gravity defining the $+Z$ axis. The $+Y$ axis is then formed from the exterior product of $Z \times X$.

The ISAS beam line consists of seven vacuum chambers that are separated by a gate valve (Fig. 1). The pressures are monitored by the vacuum gauges section by section. The primary instruments are put into two of the six chambers—a measuring chamber and an atmospheric chamber. The other chambers contain somewhat minor instruments.[10]

In this upgrade, we have introduced one large measuring chamber [Fig. 2(a)] at the downstream in which the measuring sample and detectors are installed together. The measuring chamber is cylindrical with a diameter and length of 1.8 and 11.3 m, respectively. The largeness of the measuring chamber allows us to install a detector-X stage, which changes the distance between a sample and detectors (see Sec. 2.2). In the measuring chamber, two T-type thermocouples and a contamination monitor (thermoelectric quartz crystal microbalance) are equipped, whose measuring points can be chosen arbitrarily around the upstream side of the measuring chamber. The measuring chamber is purged with dry air when the measuring sample is replaced. This procedure requires 2 to 3 h. On the other hand, bringing the chamber down to a vacuum requires 3 to 4 h to reach a level $<10^{-2}$ Pa. If dry pumps (scroll pumps) are used as a roughing pump, an extra time of 1 to 2 h is needed for this process. A pressure as low as 5×10^{-4} Pa can be realized, which takes about 1 week.

The other main chamber is the atmospheric chamber, which contains metal filters and a double-crystal monochromator (DCM) (Sec. 2.3). This chamber has been used since before

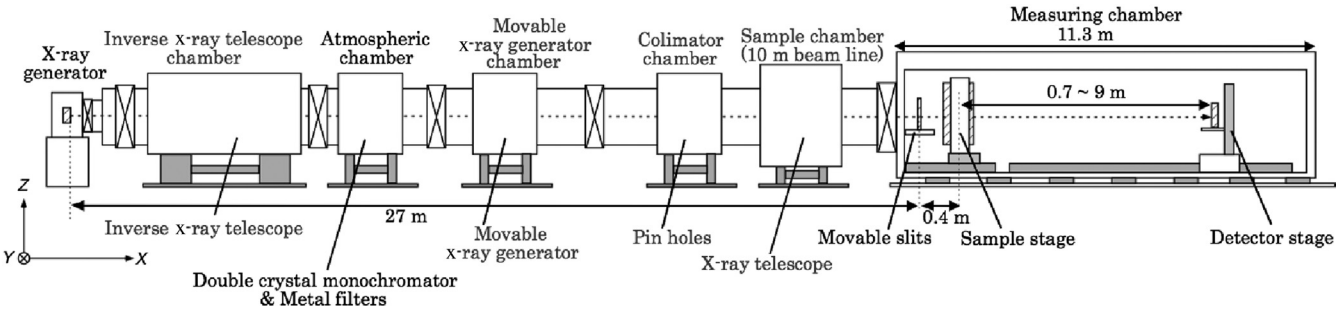

Fig. 1 Upgrated ISAS beam line. The distance between an x-ray source and the movable slit is 27 m. The total volume is separated into seven sections by six gate valves indicated by cross marks. A "measuring chamber" has been introduced whose diameter and length along the x-ray beam are 1.8 and 11.3 m, respectively. In the measuring chamber, the distance between a sample and the detectors can be changed, because the detector stage is movable along the X-axis. The details of the components described in gray on the figure are presented elsewhere.[10]

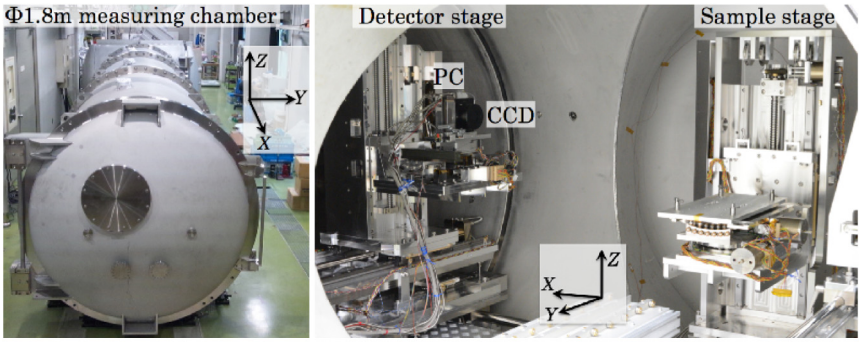

Fig. 2 (a) ϕ1.8 m vacuum chamber. (b) Sample and detector stages.

Table 1 Stage parameters.

Stages		Stroke	Default (maximum) speed	Resolution
Sample (S)	Y	−270 to 370 mm	4(5) mm s^{-1}	10 μm
	Z	±250 mm	1(1.25) mm s^{-1}	0.25 μm
	θ_Y	±5 deg	0.05(0.5) deg s^{-1}	0.0005 deg
	θ_Z	±5 deg	1(1) deg s^{-1}	0.001 deg
	θ_X	0 to 360 deg	1(1) deg s^{-1}	0.001 deg
Detector (D)	X	0 to 8.3 m	—	—
	Y	−250 to 650 mm	4(5) mm s^{-1}	10 μm
	Z	±250 mm	1(1.25) mm s^{-1}	0.25 μm
	θ_X[a]	±1 deg	0.00335(0.00335) deg s^{-1}	3.35×10^{-6} deg s^{-1}

[a]Used for alignment between detector and sample stages in rotation around X-axis.

the upgrade. The volume containing the atmospheric chamber except for the measuring chamber is usually not purged.

2.2 *Stage Systems*

The telescope and detectors are mounted on individual stages referred to as the sample stage (S stage) and the detector stage (D stage), respectively [Fig. 2(b)]. Ranges of movement, moving speeds, and resolutions of the stages are listed in Table 1. The sample stage moves the mounted telescope along the Y and Z axes, and rotates around the X, Y, and Z axes with automated controls. An x-ray CCD and a proportional counter (PC) (see Sec. 2.4) are mounted on the D stage and are automatically moved along the Y and Z axes. Moreover, the D stage can be moved by hand along the X-axis in a large range of up to 8.3 m, which enables us to choose an arbitrary distance between the sample and the detectors in the range of 0.7 to 9 m. Also, a rotational displacement around the X-axis between the S and D stages due to the movement of the D stage along the X-axis can be corrected with rotating the set of the detector stage around the X-axis ($D - \theta_X$). Note that a telescope of up to 500-mm diameter aperture can be fully scanned with the x-ray beam, because the mounted sample and the detectors can be moved in an area of 500×500 mm^2 normal to the x-ray beam.

The straightness accuracy of the move for the stages has been measured with an autocollimator. The straightness is a very important parameter when making raster measurements that are performed with the two stages moving simultaneously. Here, yawing, pitching, and rolling are defined in Fig. 3 with reference to the directions of the x-ray beam and each moving axis. Figure 4 shows the straightness as angle changes of the stages with the position of each moving axis. Note that as for the rolling of each stage (i.e., rotation around some axis with moving along that axis: $S_Y - \theta_Y$, $S_Z - \theta_Z$, $D_Y - \theta_Y$, and $D_Z - \theta_Z$), we obtained only its upper limit and it is not plotted in Fig. 4. The yawings of the S and D stages when moving along the Y ($S_Y - \theta_Z$ and $D_Y - \theta_Z$) and Z axes ($S_Z - \theta_Y$ and $D_Z - \theta_Y$) are less than 10 arc sec. Meanwhile, the pitchings of the Y-axes of the two stages ($S_Y - \theta_X$ and $D_Y - \theta_X$) are larger, and the angular changes along each axis are ~40 and ~60 arc sec for $S_Y - \theta_X$ and $D_Y - \theta_X$, respectively. The pitching of the other axes ($S_Z - \theta_X$ and $D_Z - \theta_X$) are intermediate and no larger than 30 arc sec. The upper limit of the rolling of the detector Z-axis ($D_Z - \theta_Z$) is somewhat larger and is about 60 arc sec. The limits of the rollings of other axes are 15, 20, and 25 arc sec for the sample Y-axis, Z-axis, and the detector Y-axis ($S_Y - \theta_Y$, $S_Z - \theta_Z$, and $D_Y - \theta_Y$), respectively.

2.2.1 *Beam wobbling of the raster scan*

The error of the straightness of the stage system results in "wobbling" of the image and a vignetting curve during a raster scan.[5] If the sample stage rotates by $\Delta\theta$ around an axis normal to the x-ray beam, the incident x-rays from the x-ray generator are offset by $\Delta\theta$. A vignetting curve will then be smoothed by the rotation wobbling. The different movement due to the wobbling rotation of the sample and detector stages results in a discrepancy of the $Y - Z$ position between the two stages. The discrepancy offsets the image position.

The high-accuracy straightness of the sample stage guarantees that the uncertainty of the direction of incident x-rays is

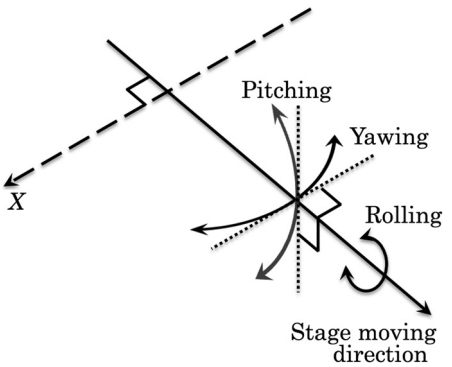

Fig. 3 Definition of yawing, pitching, and rolling. Yawing is rotation in a space containing the beam line X (see Fig. 1) direction and each moving direction. Pitching is rotation in a space containing the exterior product of the beam line X direction and the moving direction. Rolling is rotation around the moving direction.

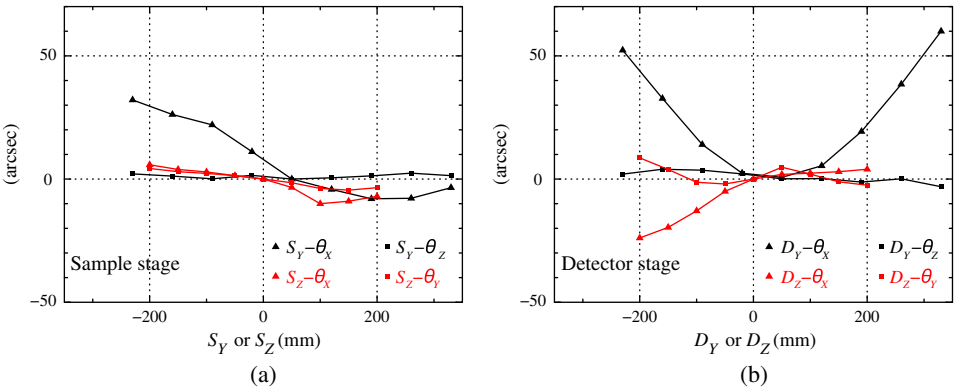

Fig. 4 Straightness of the (a) sample stage and (b) the detector stage measured with an autocollimator. Black and red correspond to the *Y*-axis and *Z*-axis of the two stages, respectively. The triangle and square show rotation around the *X*-axis (pitching) and *Z*-axis (yawing) for the *Y*-axis moving (S or $D_Y - \theta_X$ and $-\theta_Z$), respectively, and around the *X*-axis (pitching) and Y-axis (yawing) for the *Z*-axis moving (S or $D_Z - \theta_X$ and $-\theta_Y$).

20 arc sec. Measurements of the vignetting curve of the telescope can then be made with an accuracy of 20 arc sec, regardless of its focal length. For example, for ASTRO-H SXTs, whose vignetting can be reproduced by a Lorentzian function with the full width at half maximum of 16 arc min at 4.5 keV, a difference of the incident angle of 20 arc sec around the *Y*- and *Z*-axes because of the straightness causes a difference of effective area of 0.2% around the peak of the vignetting and ~4% around an off-angle of 5 arc min, where the variation of the effective area is steeper. Note that the above values regarding the effective area are maximum for cases in the SXT's aperture and are not realities when the SXT's total quality is considered. As for the detector stage, a rotation of 60 arc sec around the *Y*- and *Z*-axes is even less important, because those only result in an image shift on the detector in the order of 1×10^{-2} μm even at the maximum case where the detector stage is placed in the maximum of $+Z$.

The alignment also provides merit for telescopes with a very short focal length (<0.7 m). For a telescope with such a short focal length, the detector can also be mounted on the sample stage together with the telescope. The image wobbling at the focus is also expected to be within the alignment of 20 arc sec during a raster scan.

For a telescope with a focal length longer than 1 m, the detector must be mounted on the detector stage. The main error of the comovement of the sample and detector stages is dominated by the wobbling motion of the pitching angle along the detector's Y stage. The pitching of the Y-axis of the S stage of ~60 arc sec shifts irradiated point on a measuring telescope in *Y* direction with ~300 μm at maximum, i.e., when the stage is located at a maximum of $+Z$. This shift is not important in most cases, because a correct irradiated point on the telescope is not important for measuring the total qualities when the sample stage needs to be moved within a wide range such as above a few hundred mm. By contrast, the pitching of the detector stage of ~50 arc sec along its Y stage shifts a focusing point on detector by ~250 μm at maximum, which is consistent with a size of 11 pixels of our CCD. For example, for the ASTRO-H SXT whose focal length is 5600 mm, a focusing point shift of 250 μm corresponds to the angular wobbling of ~10 arc sec, which is almost negligible against its HPD of ~70 arc sec, although it is comparable to its point spread function (PSF) core width.

2.3 *X-Ray Beam*

In the ISAS beam line, the x-ray generator named Rigaku RU-200 has been used. The generated x-ray beam propagates through a metal filter or the DCM and is shaped into a rectangular pencil beam by a movable slit 27 m distant from the x-ray generator. The characteristics of the x-ray beam are shown in Table 2.

When x-rays are generated, a metal target is irradiated by thermal electrons with 5 to 60 keV energies. The metal targets that can be chosen are C, Al, Ti, C, Mo, W, and Pt. The metal filter for monochromating can be chosen among Al 15 μm, Ti 50 μm, or Ni 40 μm. The DCM can be used for 4 (Ti-Kα) to

Table 2 X-ray beam characteristics.

X-ray generator (Rigaku RU-200)	
Bias voltage	5 to 60 kV
Tube current	10 to 200 mA
Electron spot size (grazing size)	1×10 mm^2 (about 1×1 mm^2)
Target material	C, Al, Ti, Cu, Mo, W, Pt
Stability	~1%
Monochromator	
Metal filter	Al 15 μm, Ti 50 μm, Ni 40 μm
Ge double crystal	Used for 4 to 18 keV
Geometry	
Beam size (one side)	0.2 to 14 mm[a]
Beam divergence	8 to 115 arc sec

[a]At sample position in *x* direction

Table 3 Detector characteristics.

Proportional counter	
Window size	ϕ12 mm
Window material	15 μm aluminized mylar
Infill gas	P10 gas (Ar:90%, CH_4:10%)
Gas depth	20 mm
Energy resolution	45% (at Al-K:1.49 keV)
	30% (at Ti-K:4.51 keV)
	20% (at Cu-K:8.05 keV)
Charge coupled device	
Pixel size	22.5×22.5 μm^2
Pixel number	1240×1152
Dynamic range	16384[a], 4096[b]
Average dark current	0.3 electron pixel^{-1} s^{-1}
Read out noise	Eight electron rms
Optical blocking filter	0.5 μm aluminized polyethylene terephthalate film (Al 300 Å thick)

[a]Slow scan.
[b]High scan.

18 keV (Mo-Kα). We note that a number of metal filters or some other filters and the DCM cannot be combined.

In Table 2, the beam size is the size at the sample, which must be larger than the slit size, because the beam must have finite divergence. Therefore, the beam size is 0.2 mm at the sample even if the slit is narrowed to almost 0 mm, because of the divergence of the passed beam of 8 arc sec caused by a finite x-ray source size. For a typical case of beam size of 2×2 mm^2, the beam divergence is about 20 arc sec.

2.4 *Detectors*

The PC and CCD are mounted on the detector stage, which can be automatically replaced by each other with a dedicated stage in the vacuum. The characteristics of the two detectors are given in Table 3.

The PC has a ϕ12 mm window of 15 μm thick aluminized mylar and includes P10 gas, which consists of 90% of Ar and 10% of CH_4 by default. The included gas can be replaced by an arbitrary gas, because the PC is of the gas flow type. Figure 5 shows sample x-ray spectra acquired by the PC. Figure 5(a) is metal-filtered Al and Ti spectra in which the Kα emission lines of each element (Al-Kα: 1.49 keV and Ti-Kα: 4.51 keV) are prominent. Note that the second peak appearing in the metal-filtered Al spectrum around 7 to 8 keV is due to bremsstrahlung, which can even be resolved by energy resolution of the PC. Figure 5(b) is Cu-Kα (8.05 keV), Pt-Lα (9.44 keV), Pt-Lβ (11.07 keV), and Pt-Lγ (12.94 keV) emission lines extracted by the DCM, where the escape peaks of Ar-Kα (2.96 keV) are also prominent.

The other detector is the CCD, which is used primarily for the measurement of image qualities. The CCD measures 1240×1152 pixels of size 22.5×22.5 μm^2. The CCD is cooled down to -60°C with Peltier devices, which are also cooled down with cooling water maintained at a constant temperature of 20°C for measurements. Figure 6 is a sample of a CCD image and a 2×2 rectangular x-ray beam, whose range is from 250 to 5000 ADU and whose scale is logarithmic. Figure 7 is a projection profile. This image includes a horizontal over-clock region (504×1152 pixels on the right side) and a vertical over-clock region (1744×496 pixels on the top), which allows us to estimate both the bias level and the charge-transfer noise for each frame.

3 Example of Measurements

Here, we show an example result of the kinds of measurement that are possible with the upgraded ISAS beam line. With a light source at a finite distant from the telescope, the light focusses on a place more distant than the nominal focal length, following the lens equation. If a detector is placed at its nominal focal length, the image obtained is defocused with a width proportional to the

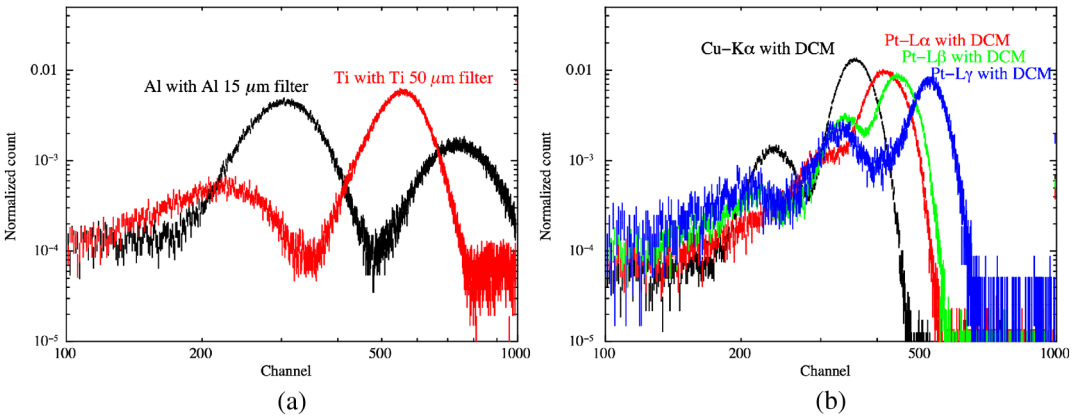

Fig. 5 X-ray spectra acquired with the proportional counter. (a) Spectra of Al (black) and Ti (red) targets with Al 15 μm and Ti 50 μm filters, respectively. The Al-Kα (1.49 keV) and Ti-Kα (4.51 keV) lines (mixture of K-α and β) make the highest peak in each spectra. (b) Spectra of Cu and Pt targets with the double crystal monochromator, which is aligned for Cu-Kα (8.05 keV, black) for the Cu target and Pt-Lα (9.44 keV, red), Lβ (11.07 keV, green), and Lγ (12.94 keV, blue) for the Pt target. Note that the amplifier gain adopted in (a) is higher than that in (b) by two times.

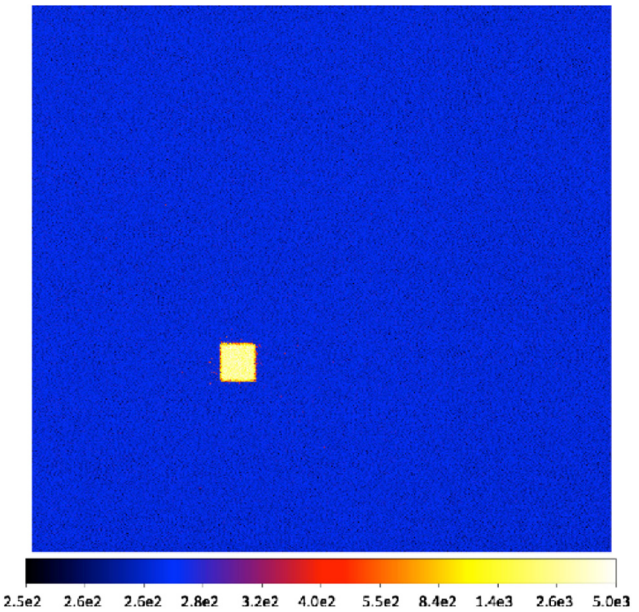

Fig. 6 Image of 2×2 mm^2 x-ray beam acquired with the CCD. Brightness is logarithmic scale from 250 to 5000 ADU. The direct image is centered at the CCD center (630,576) and extra regions on the right (504×1152 pixels) and top (1744×496 pixels) sides are a horizontal over-clock region and vertical over-clock region, respectively. Figure 7 shows the projection profiles of the direct beam, where the direct beam is quite uniform except for the edges.

used beam size. This influence is not significant for the estimation of the characteristics of rough image quality such as HPD or effective area, in general, if a thin beam such as 2×2 mm^2 is used, because these values are insensitive to the detailed image structure. By contrast, measurement of the PSF core and detailed structure of the images are significantly influenced by the defocusing. In the upgraded ISAS beam line, the distance between the sample telescope and the detectors can be chosen in the range of 0.7 to 9.0 m for each measurement. For example, the nominal focal length of the SXT onboard the ASTRO-H satellite is 5600 mm with a corrected focal length when taking into account the infinite distance from the x-ray source of 7085 mm for the ISAS beam line. Both of the focal lengths are within the allowed range. Moreover, with the corrected focal length, the beam size does not influence the sharpness of the focussed image because the rectangular beam is focused, although a size corresponding to the source size is left. This allows us to use a somewhat wider beam. However, we note that a wider beam has a larger divergent, which leads to the vignetting effect in the beam-irradiated area.

Figure 8 shows images of SXT-I[11,12] (coupled with the soft x-ray imager of the ASTRO-H), and panels (a) and (b) which were acquired with the nominal focal length and the corrected focal length. The 2×2 mm^2 beam was used for the measurement of the nominal focal length, considering defocusing proportional to the beam size and measuring time. The 2×2 mm^2 beam makes a defocusing size of ~420 μm. By contrast, the 8×8 mm^2 beam was used for the corrected focal length measurement, taking into account the vignetting effect. The incident angle to the aperture of a sample is 70 arc sec at most in this case. The field of view of the two panels of Fig. 8 is common—11.6×11.6 arc min^2, although that acquired at the nominal focal length is wider by reverse proportion to the ratio of the nominal focal length to the corrected focal length. The comparison between the two panels clearly shows that the image with the corrected focal length has more detailed structure and a sharper PSF core than those with the nominal focal length. In the corrected focal length image, the radially extended dark structures result from the alignment bars (each of which align 203 reflectors) included in the SXT. Note that even in measurement at the corrected focal length, image extension because of the finite source size must occur.

4 Summary

We upgraded the ISAS 30-m x-ray pencil beam line, where ground-based calibrations of the x-ray telescopes onboard the ASTRO-D, the ASTRO-E, the ASTRO-E2 satellites, and so on were carried out. This was done to accommodate the needs due to both the increase and decrease in the sizes of x-ray telescopes in use or planned to be used.

In this upgrade, a measuring chamber was introduced in which the measuring sample and detectors are installed together. In this chamber, the distance between the sample and the detectors can be arbitrarily set within the range 0.7 to 9 m. A measuring telescope and detectors (CCD and PC) are mounted on the sample stage and the detector stage, respectively. A telescope of up to 500-mm diameter aperture can be fully scanned with the x-ray beam without rotation of the telescope around the x-axis, because the movable range of the stages is more than 500×500 mm^2. Rotations of the two stages around the x-axes with movement along the y-axes of the sample and detector

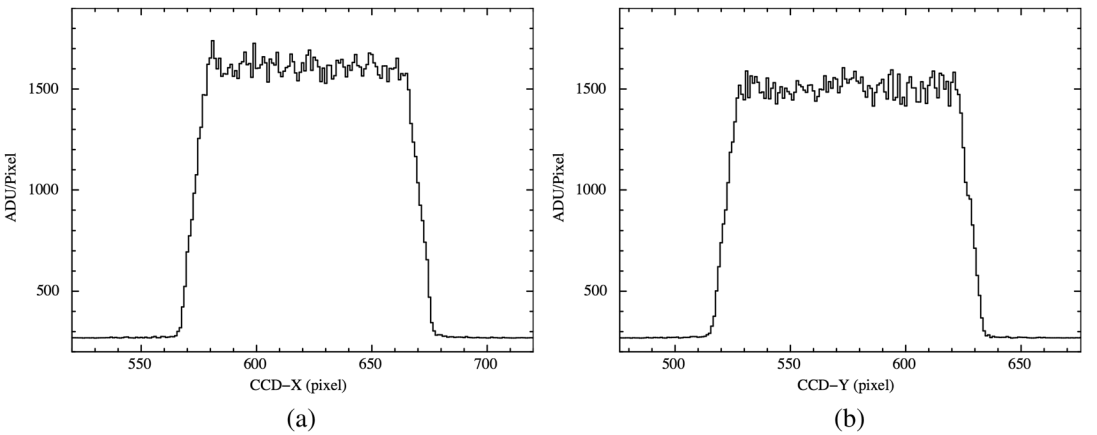

Fig. 7 Projection profiles of the direct beam to (a) *X* and (b) *Y* axes.

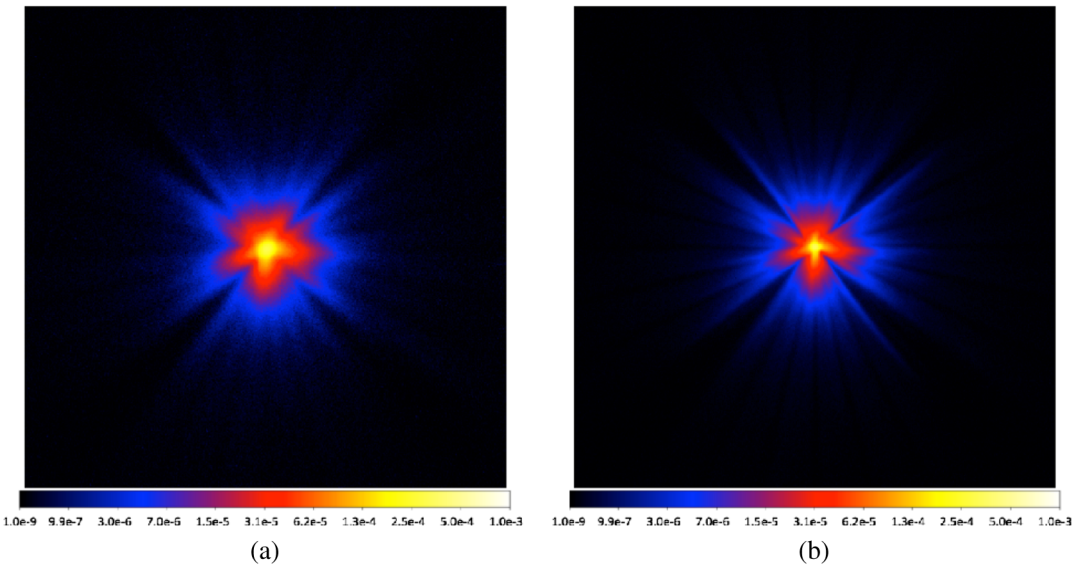

Fig. 8 ASTRO-H SXT-I images acquired with (a) 5600 mm and (b) 7085 mm of the distance between the telescope and the CCD. The distance of 5600 mm is the nominal focal length and 7085 mm is the correlated focal length, considering the beam divergence due to the finite distance from the beam source.

stages (pitching) are relatively large and change by 40 and 60 arc sec, respectively. The pitching of the other axes and the yawing of all the axes are less than 30 arc sec. As for rolling, only the upper limits were obtained because of the difficulty in measuring them. The upper limit of the detector Z axis is somewhat larger and is about 60 arc sec, while those of the other axes are less than 30 arc sec.

The x-ray from the generator is shaped into a rectangular pencil beam of 2×2 to 8×8 mm^2 by the slit 27 m distant from the x-ray generator. A metal target for the generator can be chosen among C, Al, Ti, C, Mo, W, and Pt. The DCM can be used for 4 (Ti-Kα) to 18 keV (Mo-Kα), and the metal filters of Al, Ti, and Ni can be used for any targets. The beam divergence is 20 arc sec for 2×2 mm^2 of slit width.

The PC in the ISAS beam line has a ϕ12 mm window and includes P10 gas as the default, and the CCD consists of 1240×1152 pixels of size 22.5×22.5 μm^2.

We can choose a variety of distances between the telescope and detectors for any measurement purpose. With the focal length corrected for the finite distant of the source, more detailed structure in the image can be clearly detected. Using a distance shorter than the nominal focal length gives a wider field of view.[13] We performed measurements of the ASTRO-H SXT-I images using the corrected focal length and acquired more fine-structured images and a sharper PSF core than those with the nominal focal length.

Acknowledgments

The authors are grateful to Mr. Kou Ichiharaand Mr. Kazuki Tomikawa for early phase upgrading of the beam line. Prof. Yuzuru Tawara at Nagoya University and Dr. Satoshi Sugita at Ehime University gave us an opportunity to make the thin optical blocking filter that is used in the CCD camera. Prof. Hiroshi Tsunemi at Osaka University provided us with the proportional counter. The companies, Hamamatsu Photonics K.K., Kohzu Precision Co., Ltd. and TOYAMA Co., Ltd. provided the CCD camera, the stage system, and the chambers, respectively. Mr. Chris Baluta gave us editorial support. We thank them for their efforts on production and support.

References

1. M. C. Weisskopf et al., "Chandra x-ray observatory (CXO): overview," *Proc. SPIE* **4012**, 2–16 (2000).
2. Y. Maeda et al., "Soft x-ray calibration for the NeXT x-ray telescope," *Proc. SPIE* **7011**, 70112O (2008).
3. H. Kunieda et al., "Thirty-meter x-ray pencil beam line at the Institute of the Space and Astronautical Science," *Jpn. J. Appl. Phys.* **32**, 4805 (1993).
4. Y. Tsusaka et al., "Characterization of the advanced satellite for cosmology and astrophysics x-ray telescope: preflight calibration and ray tracing," *Appl. Opt.* **34**, 4848–4856 (1995).
5. R. Shibata et al., "X-ray telescope onboard Astro-E. II. Ground-based x-ray characterization," *Appl. Opt.* **40**, 3762–3683 (2001).
6. T. Okajima et al., "Characterization of the supermirror hard-x-ray telescope for the InFOCmuS balloon experiment," *Appl. Opt.* **41**, 5417–5426 (2002).
7. P. J. Serlemitsos et al., "The x-ray telescope onboard Suzaku," *Publ. Astron. Soc. Jpn.* **59**, S9–21 (2007).
8. Y. Soong et al., "ASTRO-H soft x-ray telescope (SXT)," *Proc. SPIE* **9144**, 914428 (2014).
9. Y. Tawara et al., "Development of the four-stage x-ray telescope (FXT) for the DIOS mission," *Proc. SPIE* **9144**, 914461 (2014).
10. Y. Maeda et al., "An x-ray calibration facility with a dynamical pencil beam for the post-Astro-E2 telescopes," *Proc. SPIE* **4851**, 734–741 (2003).
11. R. Iizuka et al., "Ground-based x-ray calibration of the Astro-H soft x-ray telescopes," *Proc. SPIE* **9144**, 914458 (2014)
12. T. Sato et al., "Revealing a detailed performance of the soft x-ray telescopes of the ASTRO-H mission," *Proc. SPIE* **9144**, 914459 (2014).
13. K. Ichihara et al., "A ground calibration of the engineering model of the SXT onboard ASTRO-H using the ISAS 30 m pencil beam facility," *Proc. SPIE* **8443**, 844357 (2012).

Takayuki Hayashi was a JAXA aerospace project research associate at Institute of Space and Astronautical Science, Japan Aerospace Exploration Agency (JAXA). Currently, he is with Nagoya University as a superlative postdoctoral fellow of research fellowships for young scientists. He is a member of the ASTRO-H collaborations.

Biographies for the other authors are not available.